Supporting information for

Solvent triggered structural diversity of triple-stranded helicates: single molecular magnets†

Hongfeng Li, Peng Chen,* Wenbin Sun, Lei Zhang and Pengfei Yan*

Key Laboratory of Functional Inorganic Material Chemistry (MOE), School of Chemistry and Materials Science, Heilongjiang University, Harbin 150080, P.R. China E-mail: jehugu@gmail.com (Chen P.); yanpf@vip.sina.com (Yan P.).

Table S1 Selected bond lengths for **1**–**3** (Å).

1			
Dy1–O14	2.351(9)	Dy2–O15	2.342(9)
Dy1–O13	2.357(9)	Dy2–O4	2.345(10)
Dy1–O10	2.377(8)	Dy2–O9	2.351(10)
Dy1–O5	2.385(9)	Dy2–O8	2.374(12)
Dy1–O7	2.389(11)	Dy2–O11	2.392(9)
Dy1–O12	2.407(9)	Dy2–O6	2.411(10)
Dy1–O17	2.444(11)	Dy2–O2	2.436(10)
Dy1–O3	2.489(11)	Dy2–O1	2.496(13)
2			
Dy1–O7	2.290(5)	Dy2–O6	2.293(5)
Dy1–O3	2.351(5)	Dy2–O1	2.297(6)
Dy1–O8	2.326(5)	Dy2–O2	2.328(5)
Dy1–O4	2.348(5)	Dy2–O5	2.338(5)
Dy1–O11	2.348(5)	Dy2–O13	2.576(6)
Dy1–O15	2.474(7)	Dy2–O9	2.311(5)
Dy1–O12	2.289(6)	Dy2–O14	2.489(5)
Dy1–O16	2.484(6)	Dy2–O10	2.336(5)
3			
Dy1–O1	2.293(3)	Dy2–O3	2.297(3)
Dy1–O17	2.304(3)	Dy2–O8	2.321(3)
Dy1–O14	2.310(3)	Dy2–O15	2.321(3)
Dy1–O7	2.327(3)	Dy2–O12	2.323(3)
Dy1–O10	2.338(3)	Dy2–O4	2.326(3)
Dy1–O16	2.364(3)	Dy2–O9	2.343(3)
Dy1–O5	2.418(3)	Dy2–O2	2.425(3)
Dy1–O11	2.495(3)	Dy2–O13_#1	2.472(2)

Symmetry transformations used to generate equivalent atoms: #1 x-1,y+1,z.

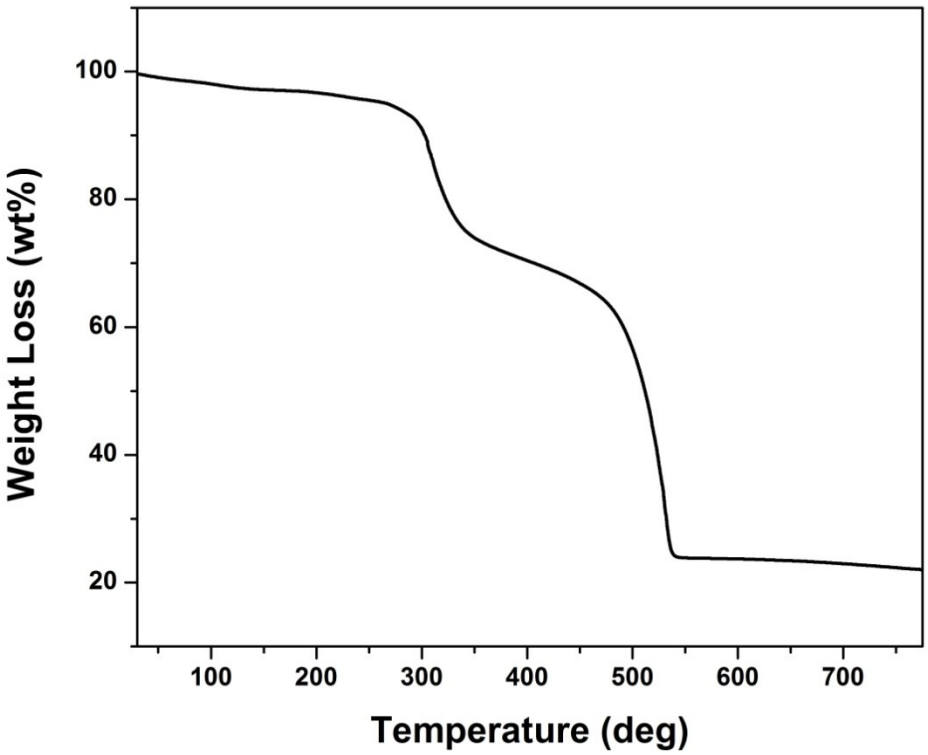

Fig. S1 TG curve of the precipitate $Dy_2(BTB)_3(H_2O)_4$.

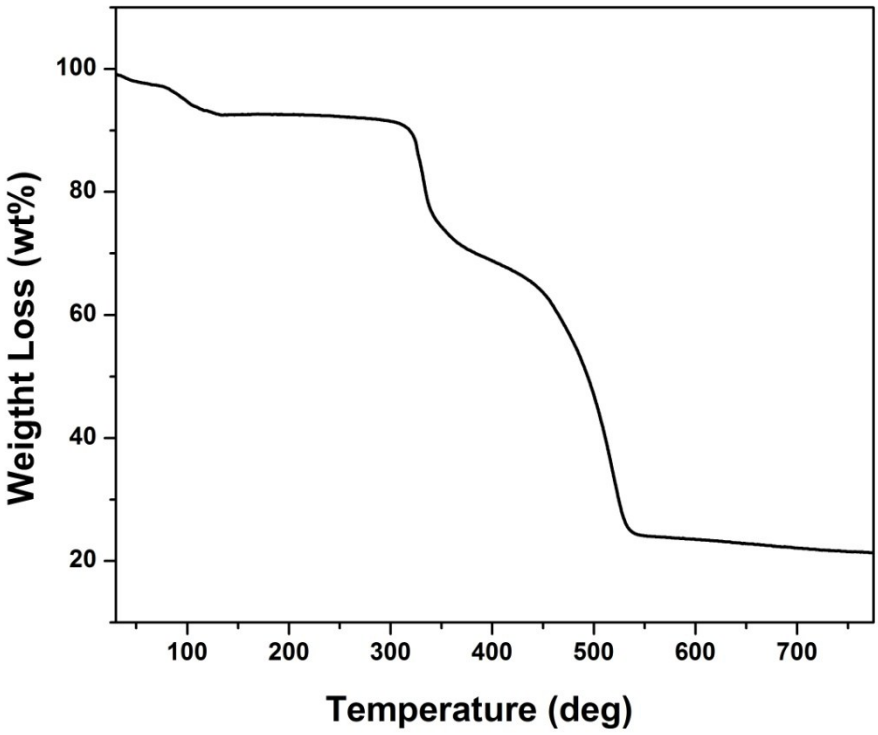

Fig. S2 TG curve of **1**.

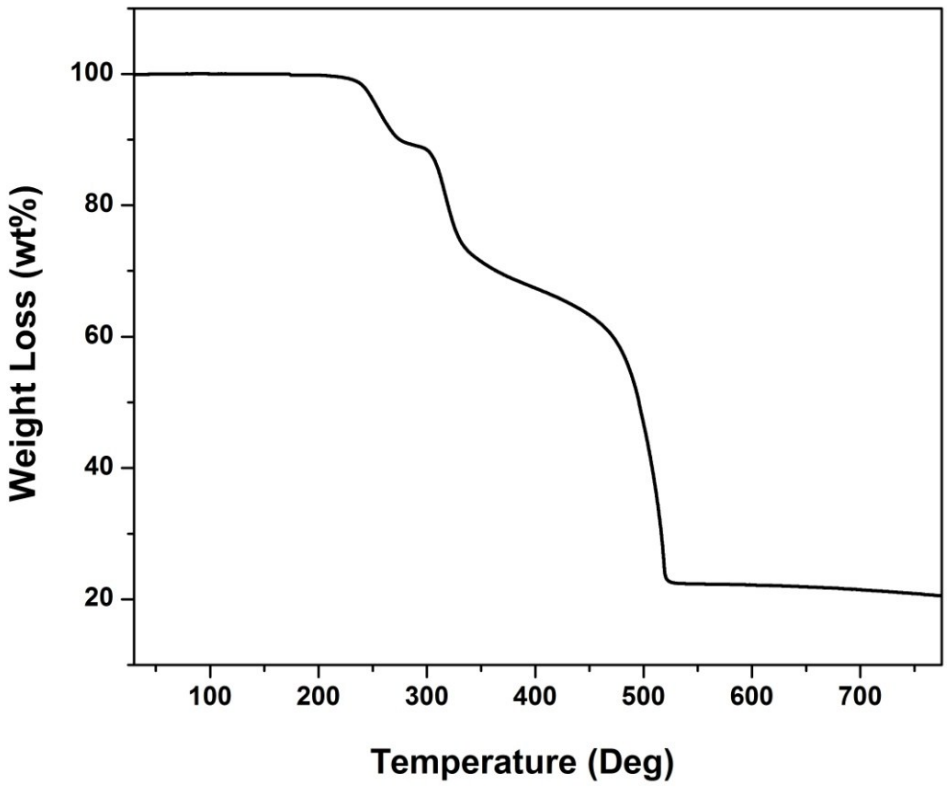

Fig. S3 TG curve of **2**.

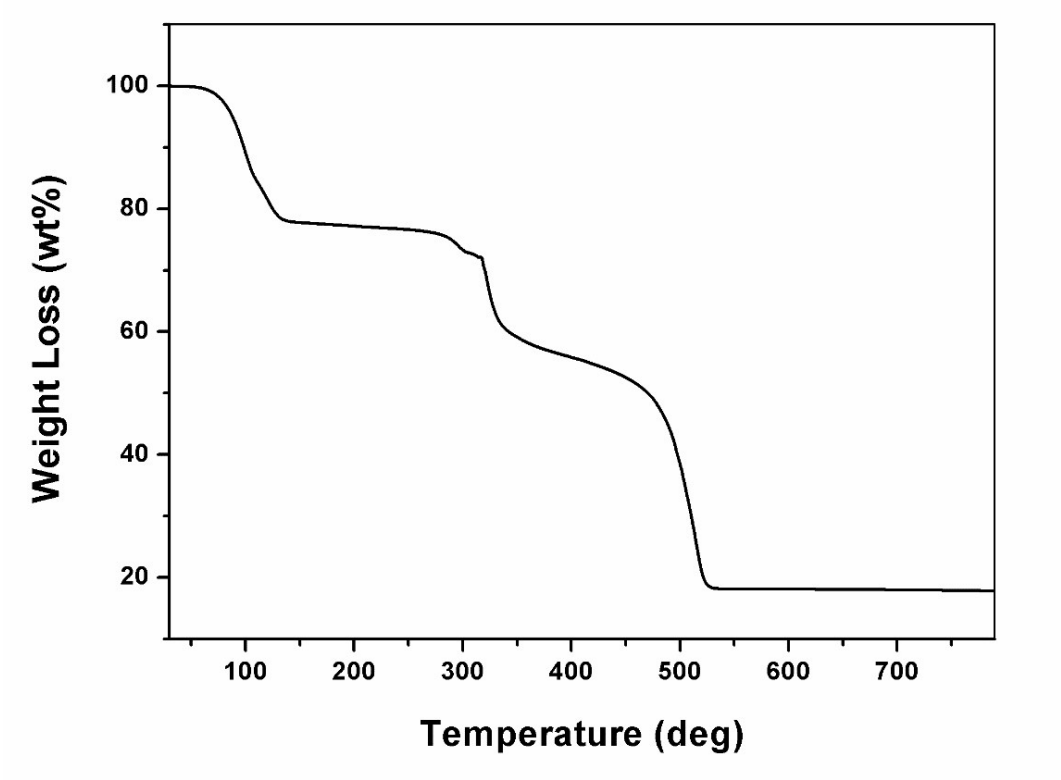

Fig. S4 TG curve of **3**.

Crystals of **1**–**3** have been selected for the thermogravimetric analysis in the experimental range of 30-780 degree, while higher temperature is unavailable because of the limitation of the equipment. TG analysis indicates a total weight loss of 79.66 wt% (calcd. 79.31 wt%) for **1**. The first stage is ascribed to the loss of methanol (found 9.06 wt%, calcd. 8.73 wt%). And the second stage occurring at 300 deg is found for the removal of one ligand until 420 deg (found 24.74 wt%, calcd. 23.35 wt%). And the third stage consequently occurring is ascribed to the removal of the rest two ligands (found 45.86 wt%, calcd. 46.23 wt%). In the case of **2**, a total weight loss of 79.49 wt% (calcd. 79.26 wt%) is observed. The first stage is ascribed to the loss of DME (found 10.31 wt%, calcd. 10.07 wt%). And the second stage occurring at 300 deg is found for the removal of one ligand until 420 deg (found 23.79 wt%, calcd. 23.81 wt%). And the third stage consequently occurring is ascribed to the removal of the rest two ligands (found 45.49 wt%, calcd. 46.62 wt%). In the case of **3**, a total weight loss of 82.13wt% (calcd. 82.49 wt%) is found. The first stage is owing to the removal of 4.5 dioxane molecules (found 18.93 wt%, calcd. 18.61 wt%) before 140 degree and a further weight loss of 1.36 wt% (calcd. 1.69 wt%) is detected for the two water molecules attached to the Dy^{3+} centers until 260 degree. Consequently, a weight loss of 4.66 wt% (calcd. 4.14 wt%) is owing to the removal of a dioxane molecule, which bridges two adjacent helicates. The fourth stage occurring at 300 deg is found for the removal of one ligand until 420 deg (found 18.29 wt%, calcd. 20.10 wt%). And the last stage consequently occurring is ascribed to the removal of the rest two ligands (found 38.89 wt%, calcd. 37.95 wt%).

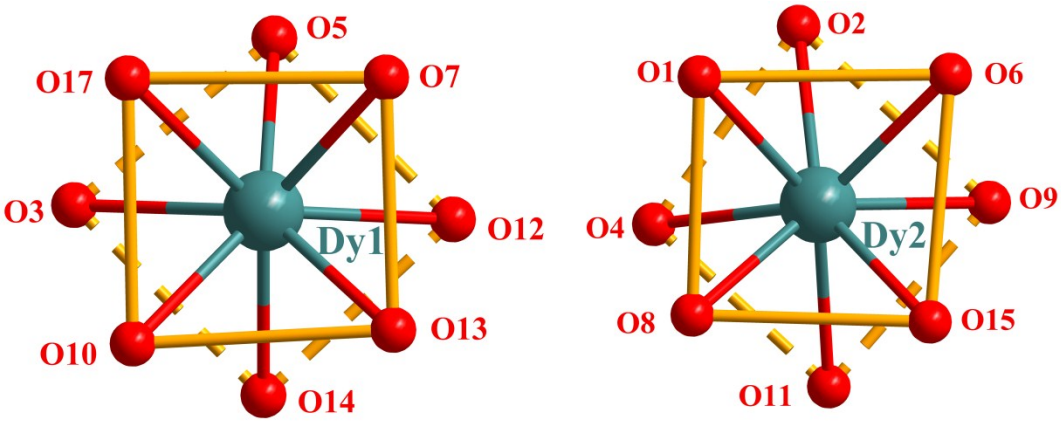

Fig. S5 The coordination geometry of Dy^{3+} ions in **1**.

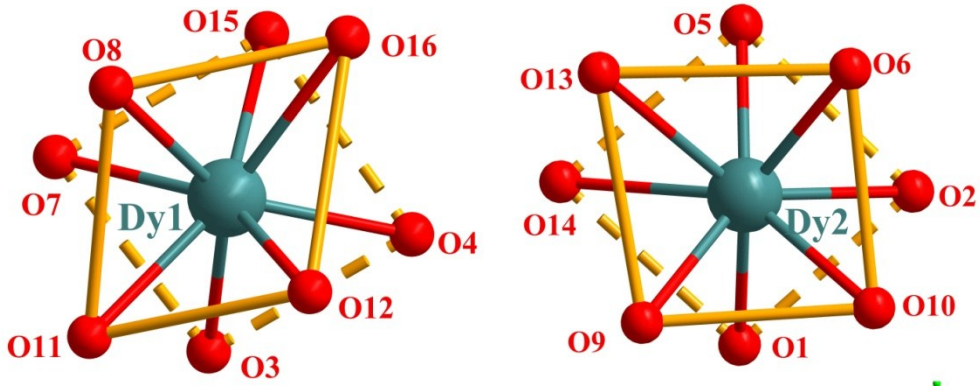

Fig. S6 The coordination geometry of Dy^{3+} ions in **2**.

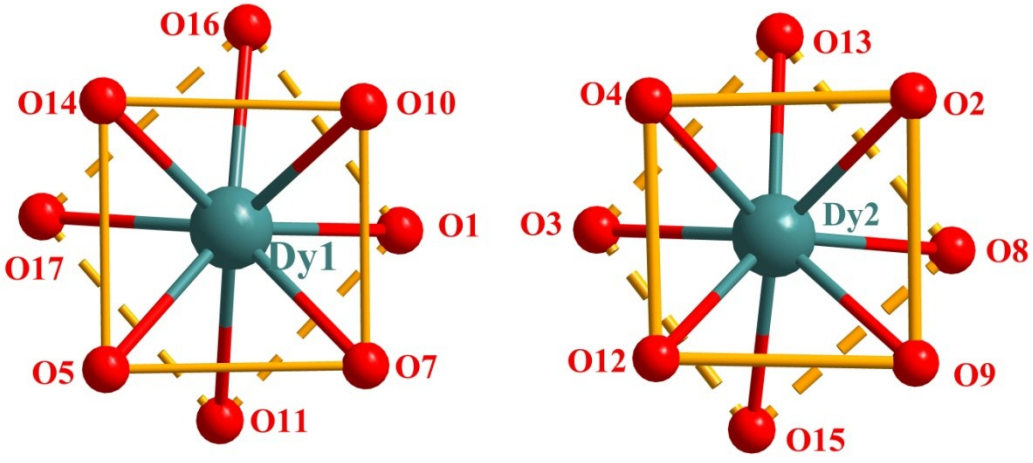

Fig. S7 The coordination geometry of Dy^{3+} ions in **3**.

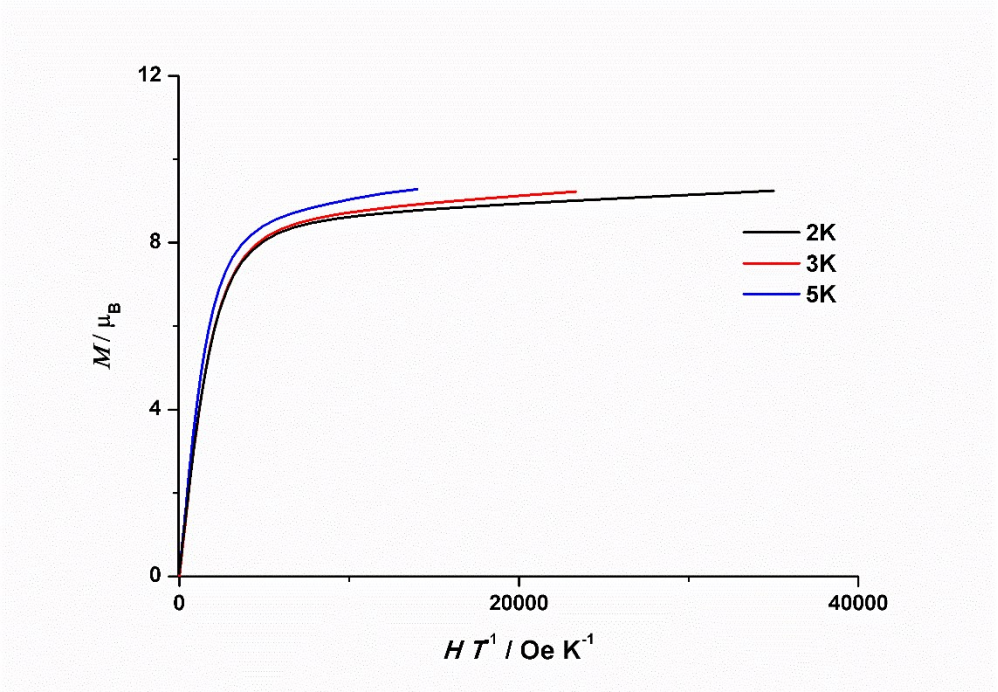

Fig. S8 Magnetization as a function of *H/T* for **1**.

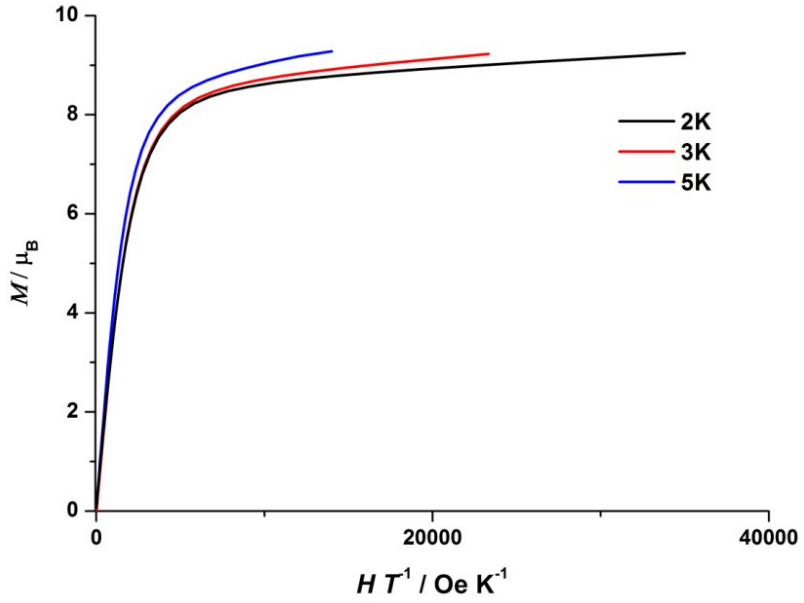

Fig. S9 Magnetization as a function of *H/T* for **2**.

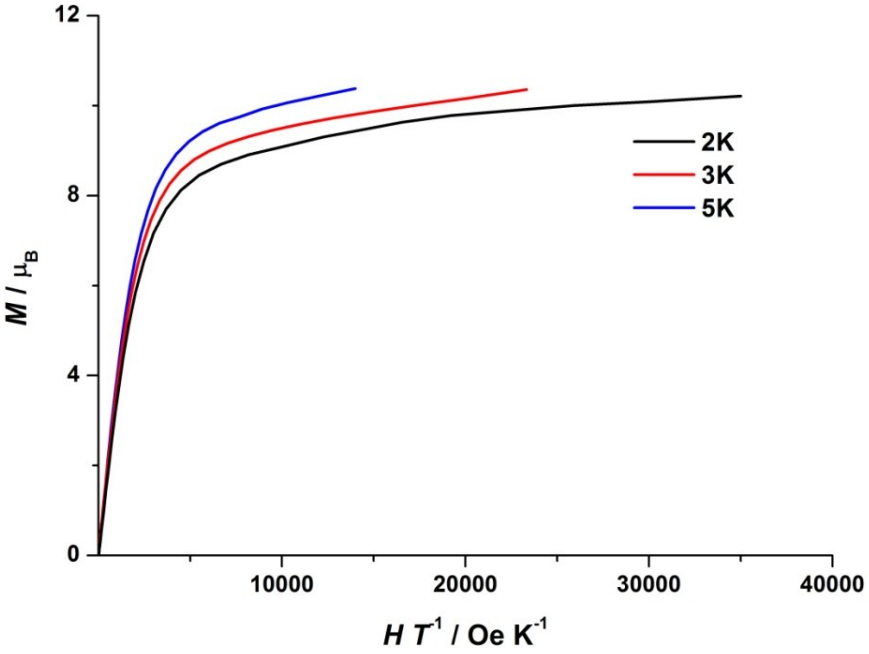

Fig. S10 Magnetization as a function of *H/T* for **3**.

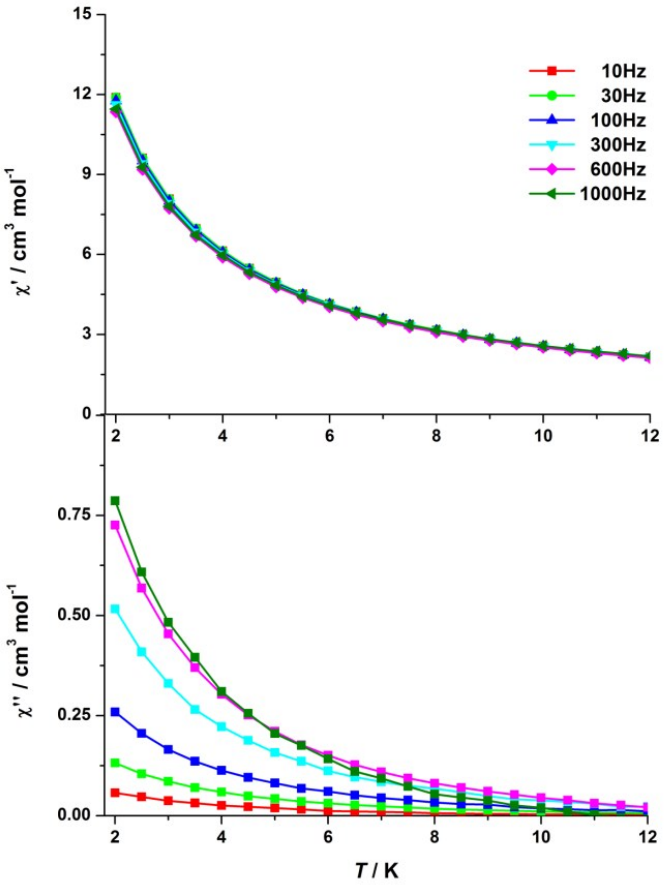

Fig. S11 Temperature dependence of the in-phase (χ', top) and the out-of-phase (χ'', bottom) ac susceptibility from 2 to 12 K under zero dc field for **1**.

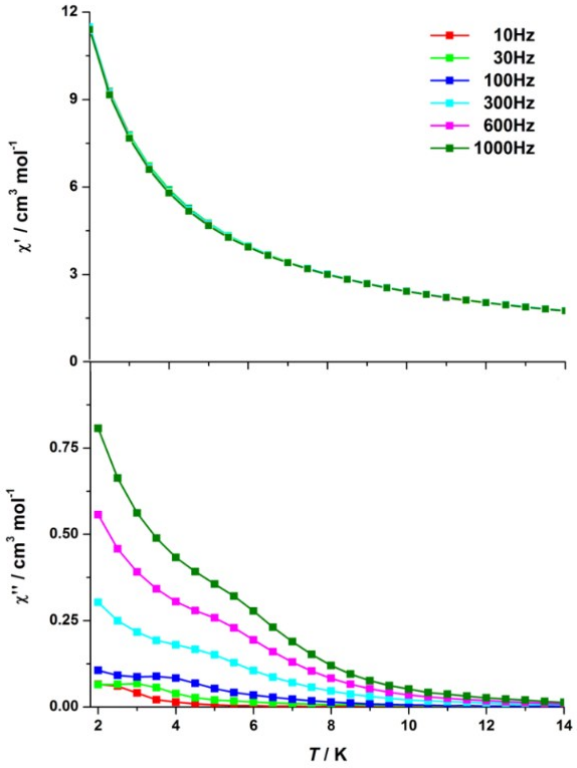

Fig. S12 Temperature dependence of the in-phase (χ', top) and the out-of-phase (χ'', bottom) ac susceptibility from 2 to 14 K under zero dc field for **2**.

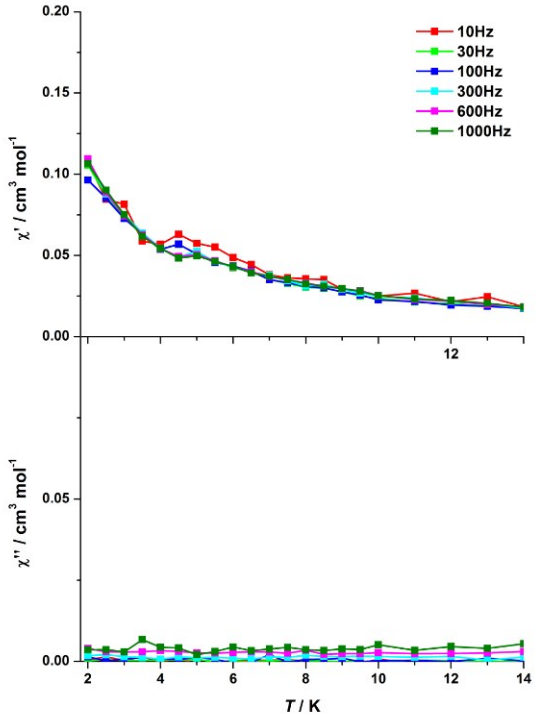

Fig. S13 Temperature dependence of the in-phase (χ', top) and the out-of-phase (χ'', bottom) ac susceptibility from 2 to 12 K under zero dc field for **3**.

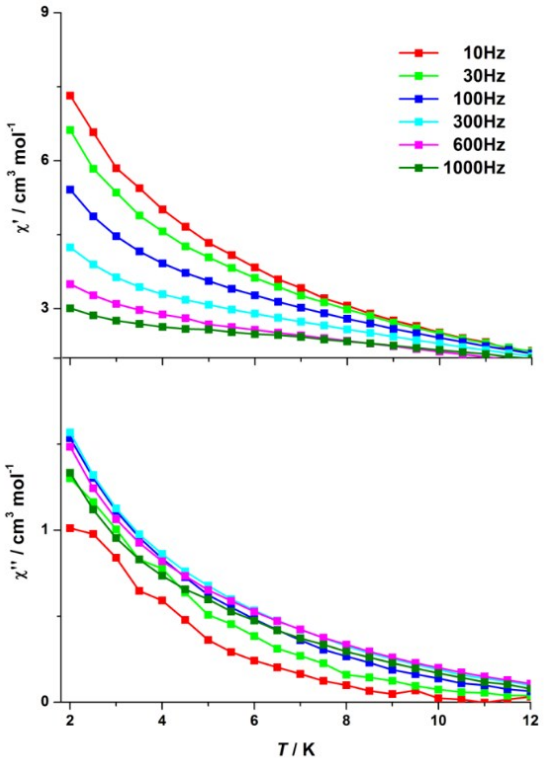

Fig. S14 Temperature dependence of the in-phase (χ', top) and the out-of-phase (χ'', bottom) ac susceptibility from 2 to 12 K under 2000 Oe dc field for **1**.

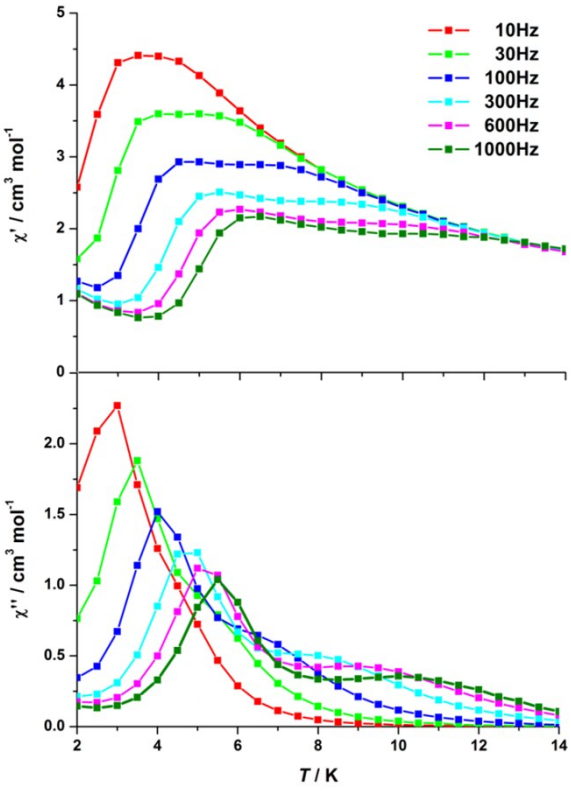

Fig. S15 Temperature dependence of the in-phase (χ', top) and the out-of-phase (χ'', bottom) ac susceptibility from 2 to 14 K under 2000 Oe dc field for **2**.

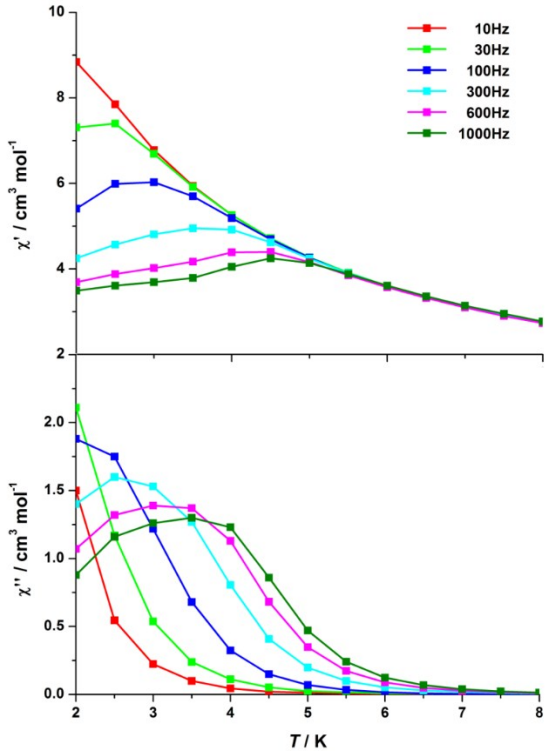

Fig. S16 Temperature dependence of the in-phase (χ', top) and the out-of-phase (χ'', bottom) ac susceptibility from 2 to 8 K under 2000 Oe dc field for **3**.

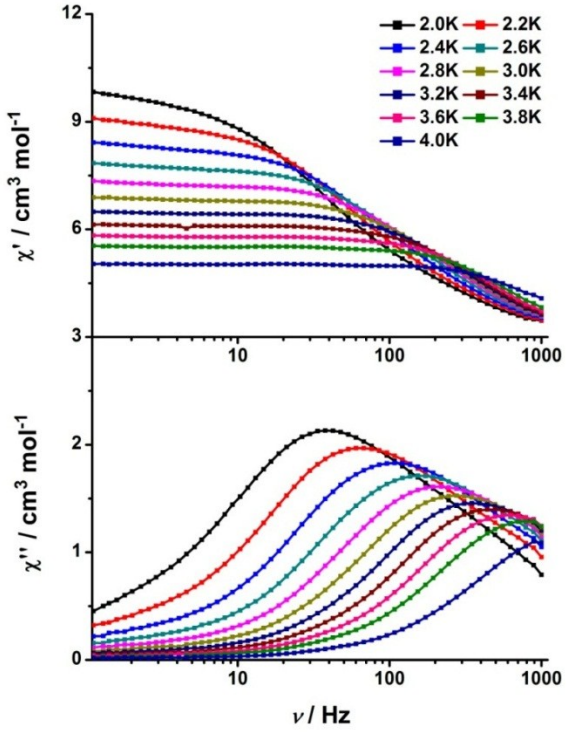

Fig. S17 Frequency dependence of in-phase (χ', top) and the out-of-phase (χ'', bottom) ac magnetic susceptibilities for **3** under an applied field of 2000 Oe in the temperature range of 2−4 K.

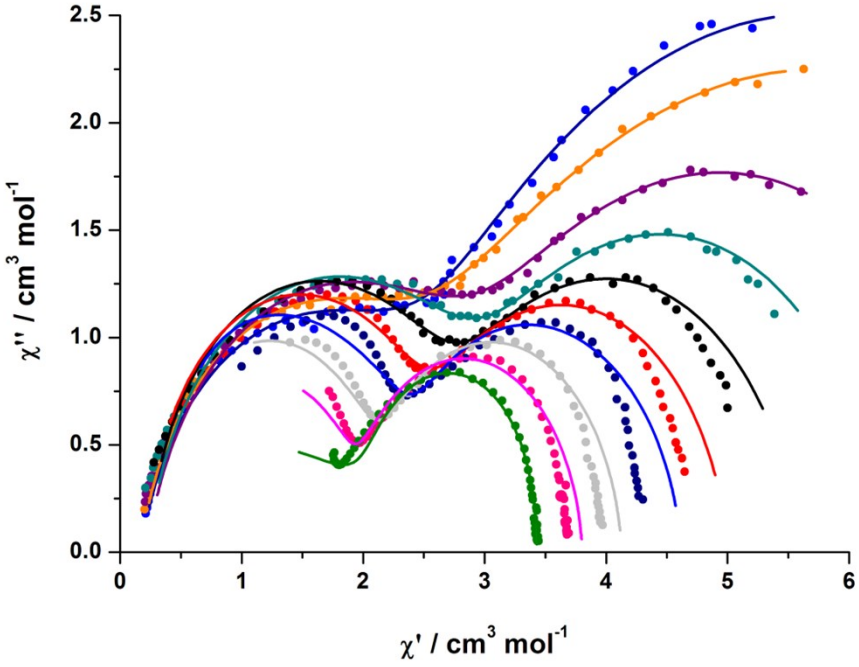

Fig. S18 Cole-Cole plots using the ac susceptibility data of **2** under an applied field of 2000 Oe (2-6.5 K, 0.5K interval).

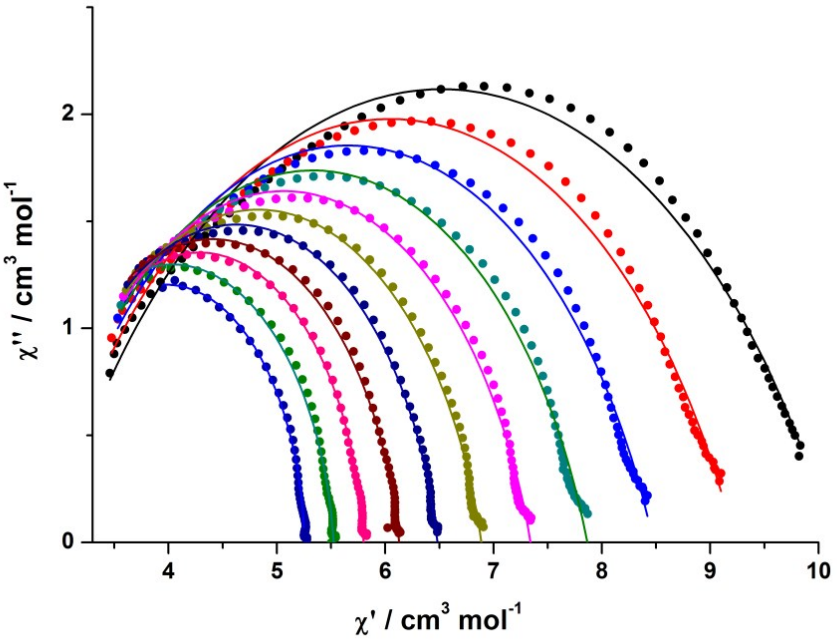

Fig. S19 Cole-Cole plots using the ac susceptibility data of **3** under an applied field of 2000 Oe (2-4 K, 0.2 K interval).